



# A study of nuclear effects in $\nu$ interactions with the NOMAD detector

M. Veltri<sup>a,\*</sup>

<sup>a</sup>Istituto di Fisica, Università di Urbino and INFN Sezione di Firenze  
V. S. Chiara 27, I-61029 Urbino, Italy

Nuclear effects in  $\nu_\mu$   $CC$  interactions with carbon nuclei have been studied by using backward going protons and  $\pi^-$ . Detailed analyses, of the momentum distributions and of the production rates, have been carried out in order to understand the mechanism producing these particles. The backward proton data have been compared with the predictions of the reinteraction and the short range correlation models.

## 1. Introduction

Since a long time [1] it has been observed that in the high energy interactions off nuclei there are particles emitted backwards, with respect to the beam direction, which have energies not allowed by the kinematics of collisions on a free and stationary nucleon. Backward going protons are commonly observed while, in absence of nuclear effects, their production is forbidden. High energy mesons, whose production in the backward direction is only allowed up to a given momentum, are detected also, at momenta above such a limit. Essentially two types of models have been proposed to explain the origin of these particles. The first is based on the intranuclear cascade (INC) mechanism. The production of particles in the kinematically forbidden region is seen as the result of multiple scattering and of interactions of secondary hadrons, produced in the primary  $\nu$ -nucleon collision, with the other nucleons while they propagate through the nucleus [2,3]. The second approach explains the production of backward particles as the result of collisions off structures with mass larger than the nucleon one. These structures are formed, at small interparticle distance, under the action of the short range part of the nuclear force. They may be described as clusters of a few correlated nucleons [4] or multiquarks clusters [5,6]. The nucleons in these structures can acquire high momenta and the fast backward going particles

can be seen as a direct manifestation of the high momentum tail of the Fermi distribution.

These two classes of models are not mutually exclusive and the production in the backward hemisphere can have contributions from both mechanisms.

## 2. The NOMAD detector and event selection

The NOMAD detector [7] consisted of an active target of 44 drift chambers,  $3 \times 3m^2$  each, of low average density ( $0.1 g/cm^3$ ) and overall mass of 2.7 tons. The drift chamber composition was made by over 90% of the total weight by carbon and elements with nearby atomic number. Downstream the beam the target was followed by a transition radiation detector which provided electron identification, a preshower and an electromagnetic calorimeter. All these systems were located inside a dipole magnet which created a magnetic field of 0.4 T. A hadron calorimeter and two muon stations were located just behind the magnet coil. NOMAD collected data from 1995 to 1998. During the run a total of  $5.1 \times 10^{19}$  protons on target, corresponding to about  $1.3 \times 10^6 \nu_\mu CC$  interactions, were recored on tape. The events are selected by requiring one primary vertex with at least two tracks, one of which has to be a negative muon of momentum greater than 3 GeV/c. The sample selected for this study amounts to 944019 events.

\*On behalf of the NOMAD collaboration

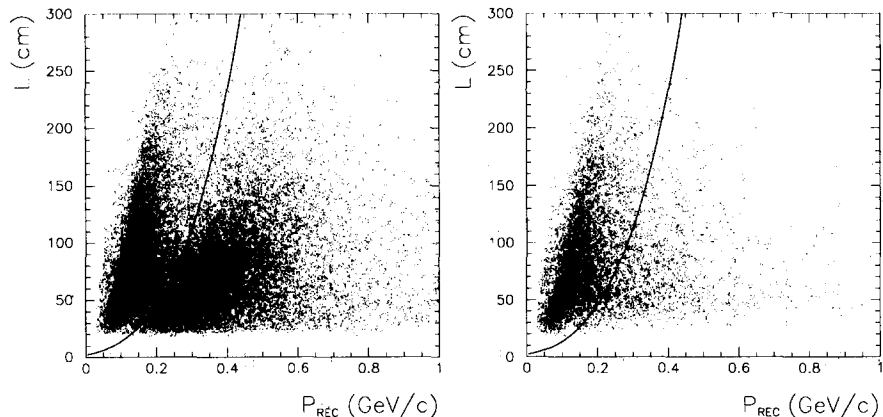


Figure 1. Distributions of length vs. momentum for positive (left) and negative (right) backward going tracks selected as described in the text. The line indicates the position of the cut.

### 3. Backward particle identification

#### 3.1. Backward proton identification

The separation of the backward going protons ( $Bp$ ) from the other backward going positive tracks (essentially  $\pi^+$ ) is done by exploiting the range-momentum relation. For this reason the candidate tracks are required to range out in the drift chamber volume. Fig. 1 shows the experimental distributions of length vs. momentum for positive (left) and negative (right) tracks, going backward with respect to the beam direction, and satisfying our selection criteria. Two distinct populations are clearly visible on the positive sample plot. Protons, having a shorter range than  $\pi^+$ , tend to accumulate in the lower right part of the plot while the  $\pi^+$ 's tend to populate the left-hand side. Comparing the two plots we see that the lower right part of the negative sample is much less populated than the corresponding region of the positive one, these tracks being mainly  $\pi^-$ . Any positive backward going track with length smaller than the cut (the line on Fig. 1) is identified as a  $Bp$ . The identified sample is then corrected for reconstruction efficiencies and for  $\pi^+$  contamination ( $\approx 8\%$  for  $P_{REC} > 250 MeV/c$ ). For further details on the identification and correction procedure refer to [8].

#### 3.2. Backward $\pi^-$ identification

In the case of backward going  $\pi^-$  ( $B\pi^-$ ) it is not necessary to look for tracks ranging out in the target. The choice of the negative charge allows for a sample of high purity; it is shown by MC studies that the  $e^-$  contamination is at the level of few percent above a momentum of  $\approx 200 MeV/c$ . We therefore assume that any negatively, backward going, charged track with  $P_{REC} > 0.2 GeV/c$  is a  $\pi^-$ . The identified sample is then corrected for reconstruction efficiency.

#### 4. Backward $p$ and $\pi^-$ invariant momentum distributions

The inclusive spectrum of backward particles is typically represented using the normalized invariant cross section  $(1/\sigma_{TOT}) E d^3\sigma/dP^3$ , where  $E$  is the energy of the backward going particle. The invariant cross section is usually parametrized by an exponential form as:

$$\frac{1}{N_{ev}} \frac{E}{P} \frac{dN}{dP^2} = C e^{-BP^2} \quad (1)$$

where  $N_{ev}$  is the total number of events,  $C$  is a constant and  $B$  is the slope parameter. Early hadronic experiments had found that  $B$  is almost independent of the projectile type and momentum, and of the atomic number of the target. This behaviour has been termed “nuclear scaling”. Neutrino experiments [9]-[13] have con-

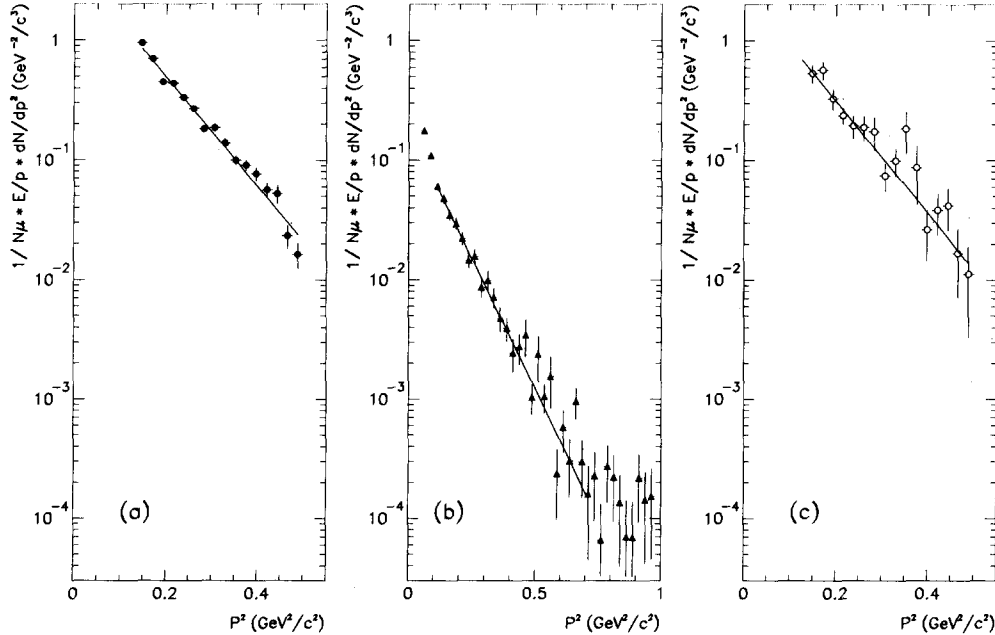


Figure 2. Invariant momentum distributions for backward going protons (a),  $\pi^{-}$  (b) in  $\nu_{\mu} CC$  events and protons in  $\bar{\nu}_{\mu} CC$  events (c)

firmed these properties.

The inclusive spectrum of  $Bp$  and  $B\pi^{-}$  is shown in Fig. 2a and 2b respectively, together with the exponential fit. In the  $B\pi^{-}$  case we have not included the first two points in the fit. These points are in a momentum region where, backward production being kinematically allowed, there are additional contributions not coming from nuclear effects. The values of the measured slope parameter  $B$  are reported in Table 1. The first and the second errors are statistical and systematical, respectively. The systematic uncertainty was estimated by slightly changing the values of all the cuts used, by varying by a small amount the correction functions and also by changing the size of the fiducial volume. The values of the slope parameters measured in this experiment are found to be compatible with the results obtained in other neutrino and hadronic experiments. The invariant cross section for  $Bp$  is larger than the one for  $B\pi^{-}$  by about one order of magnitude but the values of the slopes are similar. The kinematic

ranges of the two invariant distributions are also different. To be identified  $Bp$  have to stop inside the target volume; the rather low density of the NOMAD target restricts to  $\approx 0.7$  GeV/c the maximum useful momentum value.

The invariant cross section and slope parameter for  $Bp$  in  $\bar{\nu}_{\mu} CC$  events are given in Fig. 2c and Table 1 respectively. During normal operations  $\bar{\nu}_{\mu} CC$  events were also collected due to the small  $\bar{\nu}_{\mu}$  component of the dominantly  $\nu_{\mu}$  beam. A dedicated  $\bar{\nu}$  run yielded an additional sample of  $\bar{\nu}_{\mu} CC$  events included for this analysis.

Antineutrino events are selected under the assumptions that the efficiencies and pion contamination are the same as those used for the neutrino events, but requiring a positively charged muon instead of a negative one. The final  $\bar{\nu}_{\mu} CC$  sample consists of 61134 events.

Table 1

Fit ranges and values of the slope parameter  $B$ , for backward protons and  $\pi^-$ , as obtained from the exponential fit to the invariant cross section. The first and the second errors are statistical and systematical, respectively.

		$\Delta P$ (GeV/c)	$B(c^2/GeV^2)$	$C(c^3/GeV^2)$
Backward $p$	$\nu_\mu CC$	$0.37 \div 0.70$	$10.54 \pm 0.20 \pm 0.5$	$4.08 \pm 0.19 \pm 0.5$
	$\bar{\nu}_\mu CC$	$0.37 \div 0.70$	$10.79 \pm 0.78$	$2.71 \pm 0.54$
Backward $\pi^-$	$\nu_\mu CC$	$0.32 \div 0.85$	$10.03 \pm 0.28 \pm 0.3$	$0.17 \pm 0.01 \pm 0.02$

### 5. Energy dependence of the slope parameter

In Fig. 3 we show the slope parameter  $B$  for protons as a function of the visible hadronic energy  $E_{HAD}$  and the  $Q^2$  of the event. The visible hadronic energy is defined as:

$$E_{HAD} = \sum E_c + \sum E_n$$

where  $\sum E_c$  is the sum of the energies of reconstructed charged tracks (assuming the mass of the pion if the particle is not otherwise identified) and  $\sum E_n$  includes tracks associated to secondary vertices corresponding to interactions of neutral particles and the energy of neutral particles reconstructed in the ECAL.  $Q^2$  is the square of the four-momentum transfer,  $Q^2 = 4 E_{vis} E_\mu \sin^2 \theta / 2$ , where  $\theta$  is the muon angle with respect to the neutrino direction. No significant dependence of the slope  $B$  on either quantity is observed, in agreement with the expectations of “nuclear scaling” as observed in hadronic beam experiments. The range covered by NOMAD is similar to the one covered by different experiments with hadronic beams.

### 6. Backward particle rates

In order to study a possible atomic number dependence the  $Bp$  rate has been compared with the results of the other  $\nu$ -nucleus experiments. The measured yields have all been normalized to the same momentum interval (350 to 800 MeV/c) assuming the dependence given in Eq. 1 with the measured slopes.

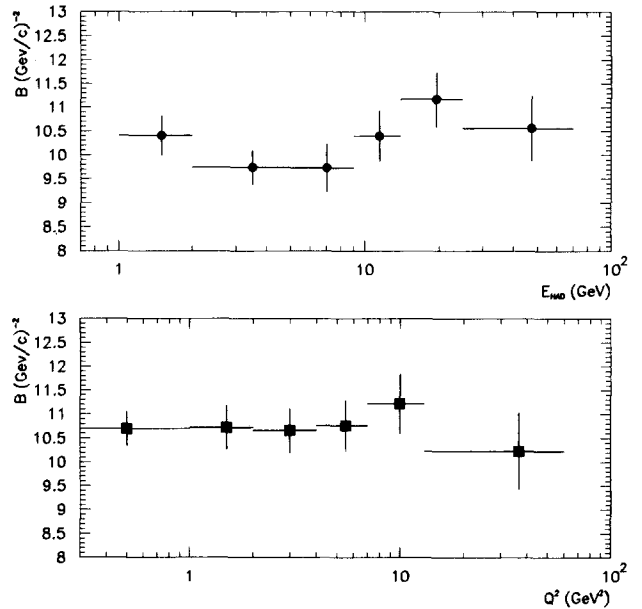


Figure 3. The value of the slope parameter  $B$  shown as a function of the hadronic energy  $E_{HAD}$  (top) and of  $Q^2$  (bottom).

The extrapolation for NOMAD gives:

$$\langle N_{Bp} \rangle_{350 \div 800 MeV/c} = [ 52.8 \pm 0.6(stat.) \pm 7(syst.) ] \times 10^{-3}$$

The  $A$  dependence for experiments most directly comparable to NOMAD is shown in Fig. 4a. In the range  $A = 20 \div 80$  it has been parametrized as  $\langle N_{BP} \rangle \propto A^\alpha$ , where  $\alpha = 0.68 \pm 0.12$  [13]. The same parametrization with a similar power law was found to describe  $Bp$  production in  $\pi^+$

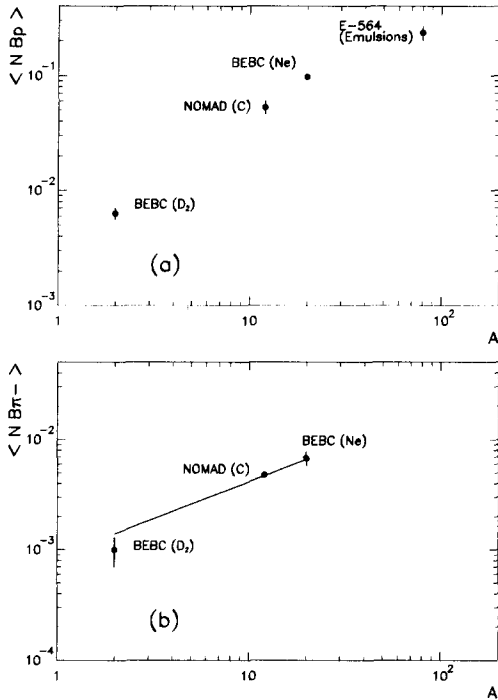


Figure 4. The average number of  $Bp$  per event (a) and of  $B\pi^-$  per event (b) in the momentum range from  $350 \div 800 \text{ MeV}/c$  in neutrino experiments as a function of the atomic number  $A$ . The line shown in (b) is the result of the fit described in the text.

and  $K^+$  collisions with  $Al$  and  $Au$  nuclei at  $250 \text{ GeV}/c$  [14]. It is evident from Fig. 4a that this simple power law does not describe the NOMAD data taken at a lower  $\langle A \rangle$ . The  $B\pi^-$  rate was directly measured in the same momentum range. Its average value is found to be:

$$\langle N_{B\pi^-} \rangle_{350 \div 800 \text{ MeV}/c} = [4.8 \pm 0.1(\text{stat.}) \pm 0.3(\text{syst.})] \times 10^{-3}$$

In this case a good fit to the two BEBC points and to the NOMAD value can be obtained using the form  $A^\alpha$  giving  $\alpha = 0.83 \pm 0.25$ , as shown in Fig. 4b.

## 7. Comparison of data with models

### 7.1. $E_{HAD}$ and $Q^2$ dependence of $Bp$ and $B\pi^-$ rates

The  $Bp$  and the  $B\pi^-$  rates have been studied as a function of the hadronic energy  $E_{HAD}$  and of  $Q^2$ . In both cases, shown in Fig. 5, a decrease of the yield with increasing  $E_{HAD}$  and  $Q^2$  is observed. This can be interpreted in terms of the “formation zone” concept. This is the distance (or the time) from the production point which is required for the secondary hadrons to be “formed”, i.e. to be able to interact as physical hadronic states. Since the distance/time required, due to the Lorentz time-dilation factor, is proportional to the energy of the secondary, the INC process is restricted to slow hadrons which have formation lengths smaller than the nuclear radius. The larger  $E_{HAD}$  and  $Q^2$ , the larger is the average energy of the outgoing partons therefore resulting in hadrons which have higher probability to be formed outside the nucleus. As a consequence, reinteractions will decrease and so will the slow proton rates. In the  $B\pi^-$  case the dependence of the yield on  $Q^2$  and on  $E_{HAD}$  is less pronounced. This can be understood since the  $B\pi^-$  rates are a less sensitive probe of nuclear effects because  $B\pi^-$  production on a stationary nucleon is kinematically allowed for momenta up to about half the nucleon mass. Furthermore  $B\pi^-$  can be produced in the decay of forward going resonances or unstable particles.

### 7.2. Effects of short range correlations in $Bp$ production

According to the picture proposed by the correlated nucleon/quark models the  $Bp$  production is explained as the result of a neutrino interaction within a correlated cluster of nucleons/quarks. This cluster is formed, for a short time, when two nucleons in their motion inside the nucleus approach each other so closely as to come under the effect of the short range component of the nuclear force ( $r_c = 0.5 \div 0.7 \text{ fm}$ ). The repulsive character of this interaction is responsible of the high relative momenta of the cluster members. The simplest, and the most probable case when considering the overlapping probabilities of nucleons

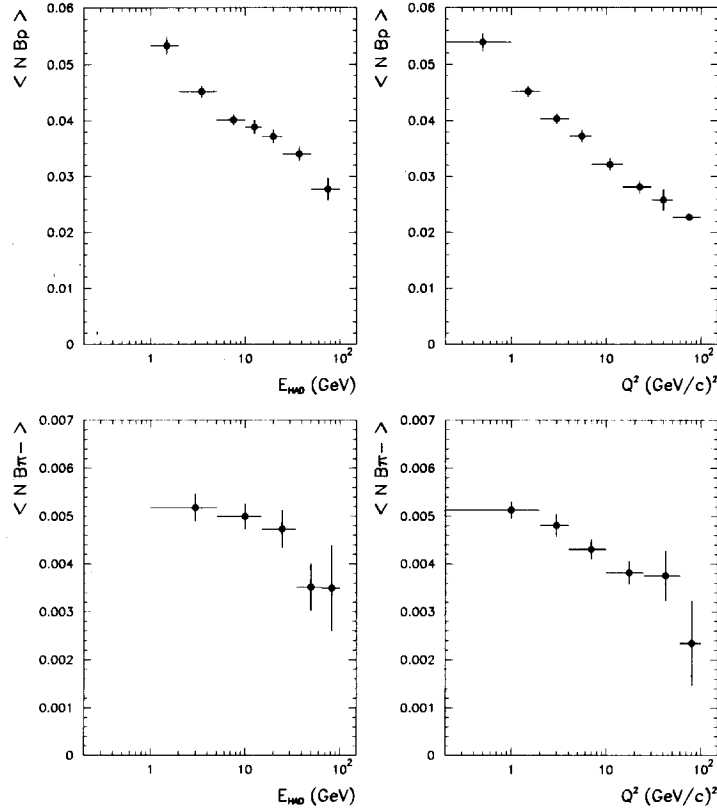


Figure 5. Top picture: the average number of  $Bp$  ( $370 < P < 700 \text{ MeV}/c$ ) per event as a function of the hadronic energy  $E_{HAD}$  (left) and of  $Q^2$  (right). Bottom picture: the average number of  $B\pi^-$  ( $350 < P < 800 \text{ MeV}/c$ ) per event as a function of the hadronic energy  $E_{HAD}$  (left) and of  $Q^2$  (right).

in the nucleus, is the two-nucleon case. According to this model the  $Bp$  is released when the correlated pair is broken in the  $\nu$ -cluster interaction. If the effects of reinteractions are neglected, the released  $Bp$  can leave the nucleus keeping its original momentum. To study these correlations it is customary to use the variable  $\alpha$  defined as:

$$\alpha = (E - P_l)/M \quad (2)$$

where  $E$  and  $P_l$  are respectively the energy and longitudinal momentum of the  $Bp$  and  $M$  is the nucleon mass. For  $Bp$ ,  $\alpha > 1$  since  $P_l$  is negative. In this model, due to the target motion a correlation between  $\alpha$  and the variable  $v = xy$ , where  $x$  is the Bjorken scaling variable  $x = Q^2/2ME_{HAD}$  and  $y = E_{HAD}/(E_{HAD} + E_\mu)$  is expected. The

variable  $v$  is related to the muon kinematics and can be written as:

$$v = (E_\mu - P_\mu^l)/M \quad (3)$$

where  $E_\mu$  and  $P_\mu^l$  are the muon energy and longitudinal momentum. The  $(v, \alpha)$  correlations were searched for in the data by calculating for each event  $\alpha$  and  $v$  as defined in Eq. 2 and 3. For each  $\alpha$  bin we plot the variable  $\langle v_N \rangle$  defined as:

$$\langle v_N \rangle = \frac{\langle v \rangle_{Bp}}{\langle v \rangle_{no\ Bp}} \quad (4)$$

where  $\langle v \rangle_{no\ Bp}$  is obtained from the full sample of events without a  $Bp$ . According to Ref. [4] the average values of  $v$  in events with a  $Bp$ ,  $\langle v \rangle_{Bp}$ , is related to the average value of  $v$  in

events where no  $Bp$  is present,  $\langle v \rangle_{no\ Bp}$ , by:

$$\langle v \rangle_{Bp} = \langle v \rangle_{no\ Bp} (2 - \alpha) \quad (5)$$

More generally for a cluster composed of  $\xi$  nucleons the relation is [6]:

$$\langle v \rangle_{Bp} = \langle v \rangle_{no\ Bp} \left(1 - \frac{\alpha}{\xi}\right) \frac{\xi}{\xi - 1} \quad (6)$$

Fig. 6a shows  $\langle v_N \rangle$  as a function of  $\alpha$ . The data indicate a slope of  $-0.22 \pm 0.06$  with a  $\chi^2/ndf = 5.3/6$  (the  $\chi^2/ndf$  in the hypothesis of no dependence on  $\alpha$  is 19.1/7). The two-nucleon correlation mechanism fails to describe our data. Either higher order structures are playing a leading role [6] or the observed low level of correlation is due to the presence of reinteraction processes. In this case part of the  $Bp$  are emitted as a result

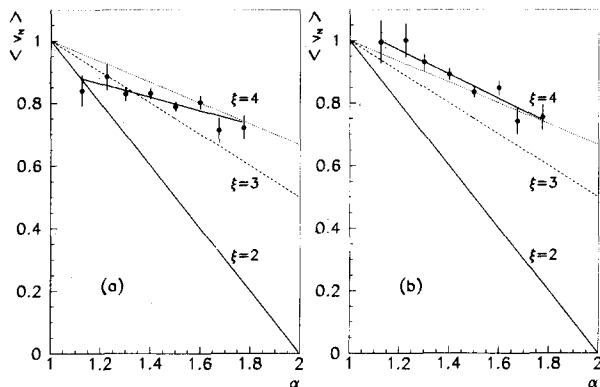


Figure 6. The variable  $\langle v_N \rangle$  plotted as a function of  $\alpha$ . The lines represent the predicted correlation (Eq. 6) for a number  $\xi$  of nucleons in the cluster equal to 2, 3 and 4. In (a) all the  $Bp$  events were used; in (b) only events having a  $Bp$  with  $\cos\theta_j < 0$ ,  $\theta_j$  being the angle of the  $Bp$  with respect to the hadronic jet direction.

of reinteractions in the nucleus and are not related to the target nucleon. The presence of intranuclear cascade processes could therefore dilute the existing correlation to the observed level. To test this hypothesis we tried to reduce the component due to rescattering in the selected  $Bp$  sample. Having observed the correlation existing between the multiplicities of slow tracks and rescattered

protons we applied increasingly tighter cuts on the number of slow tracks ( $P < 700\ MeV/c$ ). As a consequence of these cuts the degree of correlation between  $\alpha$  and  $v$  increases. The fit values of the slopes are reported in Table 2 together with the definitions of the cuts applied. We have also observed a strong correlation between the presence of protons travelling backward in the lab but forward with respect to the hadronic jet direction, and the concentration of events at small  $Q^2$  values and large angles with respect to the beam. Since also a small  $Q^2$  indicates the presence of rescattering, the exclusion of these events should highlight the expected correlation. The resulting slope is  $-0.39 \pm 0.07$  with a  $\chi^2/ndf = 4.9/6$  (see Fig. 6b). The observed behaviour is consistent with the hypothesis of the correlations effects being to some degree hidden by the presence of rescattering. Reducing the rescattering component these correlations seem to become stronger.

Table 2

The fitted value of the  $(\alpha, v)$  slope, and the corresponding  $\chi^2/ndf$ , for  $Bp$  selected from events with various numbers of positive ( $n^+$ ) and negative ( $n^-$ ) low momentum ( $P < 700\ MeV/c$ ) particles.

$n^+$	$n^-$	slope	$\chi^2/ndf$
$\leq 3$	$\leq 2$	$-0.23 \pm 0.06$	5.7/6
$\leq 2$	$\leq 1$	$-0.25 \pm 0.07$	3.3/6
$\leq 2$	0	$-0.30 \pm 0.07$	3.7/6
1	0	$-0.37 \pm 0.10$	3.9/6

## 8. Comparison with the NOMAD Monte Carlo

The NOMAD event generator NEG-N is based on a modified version of LEPTO 6.1 [15] and JETSET 7.4 [16] (with fragmentation parameters tuned on the NOMAD data) for the deep inelastic simulation and on dedicated generators for quasielastic events and events in the resonance region. Nuclear effects are taken into account by incorporating the formation zone intranuclear cascade (FZIC) code of DPMJET-II.4 [17]. For the hadrons produced inside the nucleus the code

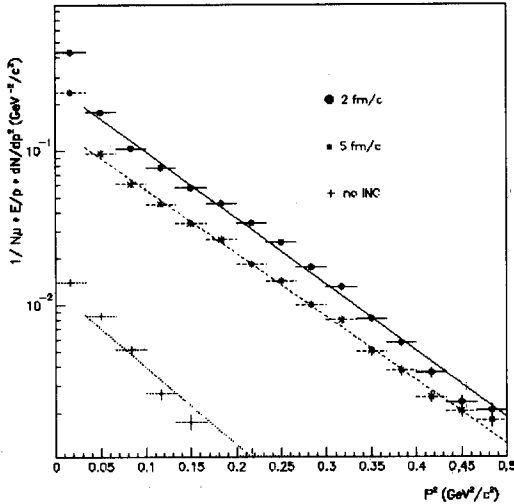


Figure 7. Invariant momentum distributions of  $Bp$  simulated with  $NEG-N$  for different values of the formation time parameter.

performs a complete simulation of tracking and of interactions in nuclear matter developing the cascade through several generations. The Fermi momentum is simulated according to [18]. The event generator used for the oscillation search did not take into account the INC. In that case a discrepancy of  $200 MeV/c$  on the average transverse missing momentum,  $p_T^m$  (the difference between the reconstructed hadron jet and muon transverse momenta), was found between the data and the MC prediction. In view of its importance in the  $\tau$  search, based on the exploitation of the different kinematics of the  $\nu_\tau$  interactions with respect to the  $\nu_e$  and  $\nu_\mu$  ones in the transverse plane, the MC sample could not be directly used to calculate background and signal efficiencies. However, a method [19] was successfully developed in order to correct the MC predictions using the data themselves. The results of this upgraded generator show how the INC degrades the hadronic energy by producing  $n$  and slow  $p$  (emitted at large angles and difficult to detect). The simulation of nuclear effects reduces by a factor of two the  $p_T^m$  discrepancy between data and MC; the remaining effect is probably due to a too optimistic detector simulation. In the code the hadron formation length is left as a free parameter to be supplied by the user. It has been tuned on the

NOMAD data in order to achieve the best agreement between the simulated and the experimental hadronic distributions of multiplicities, momentum spectra and angular distributions. The best agreement is found for a formation time of  $2 fm/c$ . For this value the MC predicts a rate of  $\langle N_{Bp} \rangle_{350 \div 800 MeV/c} = 53.0 \times 10^{-3}$  with a slope of 10 in excellent agreement with the experimental results. It was found also (see Fig. 7) that the rate is strongly dependent on the formation time while the slope is not.

## REFERENCES

1. A. Baldin et al., Sov. J. Nucl. Phys. **18** (1973) 41.
2. V. B. Kopeliovich, Phys. Rep. **139** (1986) 51.
3. A. Ferrari et al., Z. Phys. **C 70** (1996) 413.
4. L. L. Frankfurt and M. Strikmann, Phys. Lett **B 69** (1977) 93; Phys. Rep. **76** (1981) 215.
5. C. E. Carlson, K. E. Lassila and U. P. Sukhatme, Phys. Lett. **B 263** (1991) 277.
6. L. A. Kondratyuk and M. Zh. Shmatikov, Z. Phys. **A 321** (1985) 301.
7. J. Altegoer et al. NOMAD Coll., Nucl. Instr. and Meth. **A 404** (1998) 96.
8. P. Astier et al. NOMAD Coll., Nucl. Phys. **B 609** (2001) 255.
9. J. P. Berge et al., Phys. Rev. **D 18** (1978) 1367; V. I. Efremenko et al. Phys. Rev. **D 22** (1980) 2581.
10. A. A. Ivanilov et al., JETP Lett. **30** (1979) 362.
11. V. V. Ammosov et al., Sov. J. Nucl. Phys. **43** (1986) 759.
12. E. Matsinos et al. Z. Phys. **C 44** (1989) 79.
13. M. Dayon et al. Z. Phys. **C 56** (1992) 391.
14. N. M. Agababyan et al, EHS/NA22 Coll., Z. Phys. **C 66** (1995) 385.
15. G. Ingelman, LEPTO 6.1, in Proc. of Physics at HERA, DESY, Hamburg (1992) 1366.
16. T. Sjöstrand, Computer Phys. Commun. **39** (1986) 347.
17. J. Ranft, Gran Sasso Lab. Report, INFN/AE-97/45 (1997).
18. O. Benhar, private communication.
19. J. Altegoer et al., NOMAD Coll., Phys. Lett **B 431** (1998) 219.